JACS
JOURNAL OF THE AMERICAN CHEMICAL SOCIETY

ARTICLE

pubs.acs.org/JACS

Self-Assembly of a Donor−Acceptor Nanotube. A Strategy To Create Bicontinuous Arrays

Siyu Tu,[†] Se Hye Kim,[†] Jojo Joseph,[‡] David A. Modarelli,[*,‡] and Jon R. Parquette[*,†]

[†]Department of Chemistry, The Ohio State University, 100 West 18th Avenue, Columbus, Ohio 43210, United States

[‡]Department of Chemistry and Center for Laser and Optical Spectroscopy, The University of Akron, Akron, Ohio 44325-3601, United States

Supporting Information

ABSTRACT: The self-assembly of bolaamphiphile **1** into nanotubes containing a nanostructured electron donor/acceptor heterojunction is reported. In 10% MeOH/H_2O, the tetraphenylporphyrin (TPP) and 1,4,5,8-naphthalenetetracarboxylic acid diimide chromophores engage in strong *J*-type $\pi-\pi$ interactions within monolayer rings that further stack into the nanotube assemblies. In 10% MeOH/H_2O at pH 1 or 11 or in pure MeOH, assembly is driven exclusively by the TPP ring, leading to the formation of nonspecific, unstructured aggregates. Steady-state, time-resolved fluorescence and femtosecond transient absorption spectroscopy revealed a strong dependence of the fluorescence decay and electron-transfer/charge-recombination time constants on the nature of the assemblies. These studies highlight the importance of local nanostructure in determining the photophysical properties of optoelectronic materials.

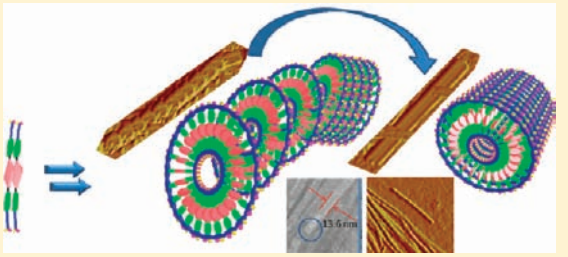

INTRODUCTION

Controlling the structure of the electron donor/acceptor (D/A) interface in charge-separating materials at a molecular level is critical for the development of thin-film optoelectronics as a viable alternative to silicon-based materials.[1] Interpenetrating phase-separated D/A blends (bulk heterojunctions) have made significant progress toward this goal, but the structure and dimensions of the D/A interface are difficult to control in these blends.[2] The self-assembly of organic π-systems has recently emerged as a method to create nanostructured *p*-type or *n*-type materials.[3] The cofacial π-stacking interactions that often comprise such nanostructures are expected to produce maximal charge carrier mobilities.[3b,4] Ideal materials for charge separation would maintain separate π-conjugated pathways for both the donor and acceptor chromophores within a single nanostructure. Hence, the self-assembly of D/A dyads has received recent attention as a method to tune the nanostructure of D/A interfaces.[5] Despite the exceptional electronic characteristics of carbon nanotubes,[6] nanotubular assemblies of D/A dyads remain exceptionally rare.[7] Herein, we present the bolaamphiphilic self-assembly and photophysical properties of a tetraphenylporphyrin (TPP)−1,4,5,8-naphthalenetetracarboxylic acid diimide (NDI) nanotube.

Previously, we reported an NDI−dilysine bolaamphiphile that assembled into nanotubes via the stacking of intermediate monolayer lipid nanorings.[8] The presence of *J*-type intermolecular $\pi-\pi$ interactions between adjacent NDI chromophores in the monolayer mediated facile energy migration along the NDI stacks. To explore the applicability of this strategy for the assembly of D/A nanotube arrays, we constructed an analogous bolaamphiphile comprised of a central porphyrin chromophore flanked on both ends by NDI−lysine moieties. We reasoned that the potential for porphyrins to engage in strong intermolecular $\pi-\pi$ interactions should drive the assembly process.[9] The symmetrical design of the bolaamphiphile was intended to preclude the potential for antiparallel packing in the membrane that would give rise to, or result from, D/A charge-transfer complexation. However, this design significantly increases the hydrophobic/hydrophilic ratio of the molecule compared with NDI−dilysine,[8] an important factor in determining the nature of the assembly.[10] Remarkably, we found that this bolaform design extends to bolaamphiphile **1**.

EXPERIMENTAL SECTION

Synthesis of Bolaamphiphile 1. Bolaamphiphile **1** was prepared by reaction of 5,15-bis(4-aminophenyl)-10,20-diphenylporphyrin (**2**)[11] with 2 equiv of the *N*-Boc-L-lysine monoimide **3**. Monoimide **3** was accessed via monoimidation of 1,4,5,8-naphthalenetetracarboxylic dianhydride with *N*-Boc-L-lysine. Deprotection with TFA/$(C_2H_5)_3SiH$ in CH_2Cl_2 produced **1** as a purple solid after purification by reverse-phase high-performance liquid chromatography (Scheme 1). Although bolaamphiphile **1** was soluble in common organic solvents, the addition of 10% methanol was necessary for dissolution in aqueous media.

Nanotube Self-Assembly. Transmission electron microscopy (TEM) of a fresh, negatively stained sample of **1** in 10% MeOH/H_2O (5 mM) revealed the formation of well-organized, micrometer-long nanotubes with diameters of 13.6 nm and wall thicknesses of 4.6 nm (Figure 1a). The wall thickness corresponds with the extended length of **1** (~4.6 nm), consistent with a monolayer wall structure. A few nanotubes

Received: June 23, 2011
Revised: September 29, 2011
Published: October 17, 2011

Scheme 1. Synthesis and Structure of Bolaamphiphile 1

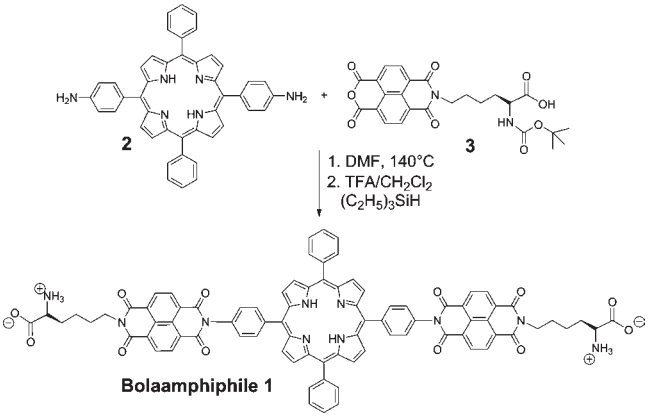

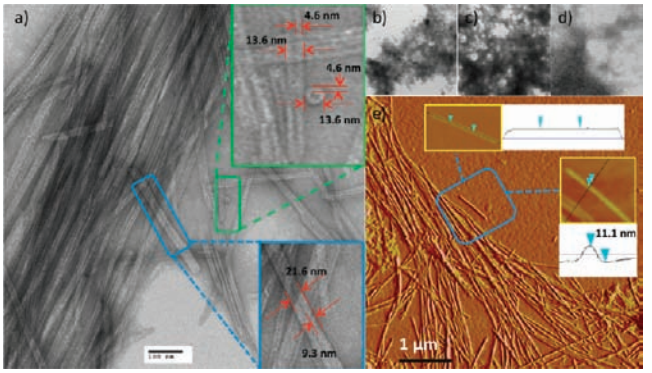

Figure 1. Bolaamphiphile **1**. TEM image (5 mM, carbon-coated copper grid) with 2% (w/w) uranyl acetate as negative stain of fresh samples of **1** in 10% MeOH/H_2O (a) at pH 7 (inset: nanotubes and nanorings with dimensional analysis), (b) at pH 1, (c) at pH 13, and (d) in pure MeOH. (e) Tapping-mode AFM image on freshly cleaved mica (5 mM) (inset: nanotube dimensional analysis and surface analysis).

with larger diameters, ranging from 21.6 to 70.2 nm, and 2- to 7-fold thick walls comprised of multiple monolayers were also present (Figures 1a, S1).[10c,12] After aging for 2−3 days, a filamentous, thread-like precipate formed, which contained a greater proportion of larger nanotubes than the fresh sample. The nanotubes appeared as two white, parallel lines separated by a darker center, which is consistent with the cross-sectional view of a hollow tubular structure filled with the negative stain, uranyl acetate.[13] Nanorings with the same dimensions as the nanotubes and the open end of the tubes were occasionally observed by TEM imaging (Figures 1a inset and S1). In contrast to 10% MeOH/H_2O, no discernible assemblies could be observed in 2,2,2-trifluoroethanol (TFE) by TEM. Amorphous aggregates were formed at pH 1 and 13 in 10% MeOH/H_2O and in pure MeOH (Figure 1b−d).

Tapping-mode atomic force microscopy (AFM) images of **1** on mica similarly revealed high-aspect-ratio assemblies with cross-sectional heights of 11.1 nm (Figures 1e and S2). Closer inspection of the larger nanotubes present in the AFM images revealed that they were comprised of nanorings stacked columnar-like on top of one another (Figures 2a, S3, and S4). The nanoring stacks then fused together into tubes with smooth surfaces (Figure 2c,d). The progression from stacks of discrete rings to completely formed nanotubes with smooth surfaces was also observable. A self-sorting assembly process whereby only nanorings with identical dimensions stack together to form nanotubes was apparent in Figure 2b. Accordingly, short stacks of identically sized

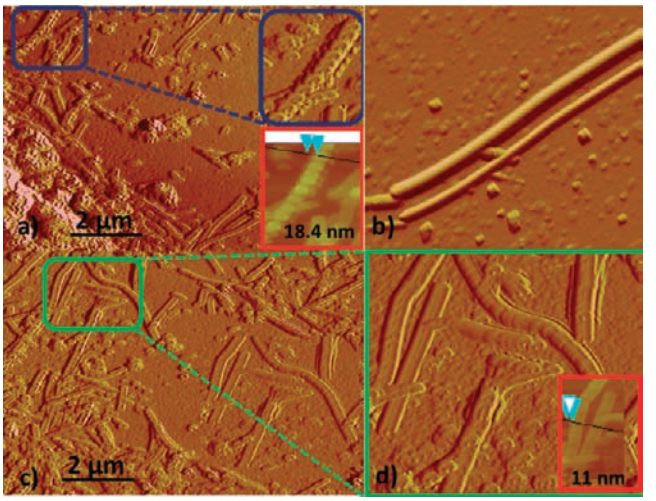

Figure 2. Tapping-mode AFM images of **1** (5 mM, 10% MeOH/H_2O, pH 7) on freshly cleaved mica, showing the progression from stacked nanorings to fully formed nanotubes.

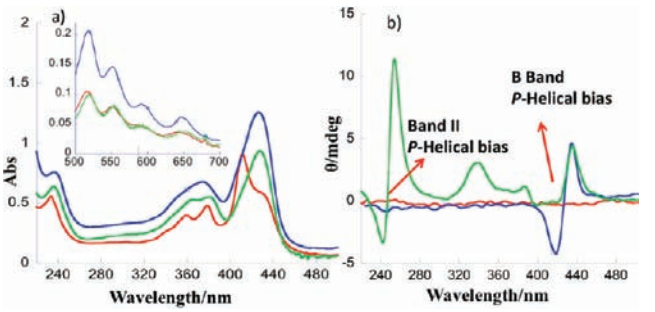

Figure 3. (a) UV spectra (inset: porphyrin Q-bands) and (b) CD spectra (50 μM) in TFE (red), MeOH (blue), and 10% MeOH/H_2O (green).

rings along with two complete nanotubes having discrete, uniform diameters were present in the image.

DISCUSSION

***J*-Type $\pi-\pi$ Aggregates.** In TFE, in which **1** remains predominantly monomolecular, the absorption spectrum exhibited peaks at 232 nm and from 350 to 400 nm, corresponding to bands II and I, for the NDI chromophore, respectively, and at 409 nm due the porphyrin Soret band. The shoulder at ~428 nm in TFE reflects the occurrence of a small amount of aggregation that is not apparent in the TEM images. Red-shifting of the Soret band (427 nm) and of the NDI bands in 10% MeOH/H_2O is consistent with the presence of *J*-type $\pi-\pi$ interactions of both the porphyrin[14] and NDI chromophores[15] within the nanotubes (Figure 3a). Likewise, the formation of the amorphous aggregates at pH 1 and 13, and in pure MeOH, was accompanied by broad, red-shifted peaks (Figure S6). However, these conditions produced characteristically different circular dichroism (CD) spectra compared with those obtained in 10% MeOH/H_2O. Notably, the CD spectrum of **1** in 10% MeOH/H_2O showed Cotton effects between 300 and 400 nm due to band I of the NDI chromophore along with strong positive excitonic couplets centered at ca. 240 and 428 nm, corresponding to NDI (band II) and porphyrin (Soret band) transitions, respectively (Figure 3b).

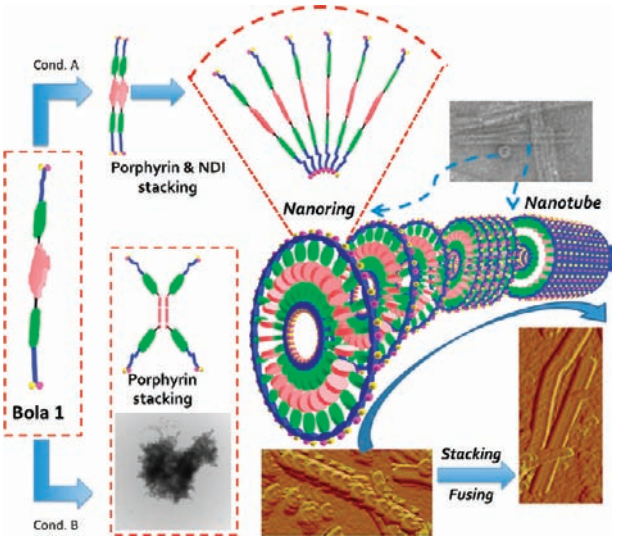

Figure 4. Schematic representation of the self-assembly of bolaamphiphile **1**. In 10% MeOH/H_2O (conditions A), **1** undergoes self-assembly into monolayer nanorings, which further stack into nanotubes. In pure MeOH, or at pH 1 or 11 in 10% MeOH/H_2O, porphyrin-driven nonspecific aggregation occurs (conditions B). TEM images show (top right) nanotubes and nanorings and (bottom left) nonspecific aggregates (10% MeOH/H_2O, pH 1), and a portion of the AFM image (bottom right) shows the supramolecular stacking of nanorings into nanotubes.

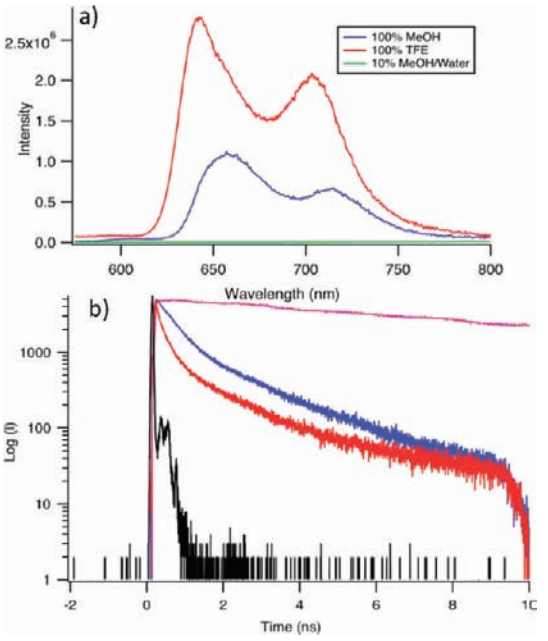

Figure 5. (a) Steady-state fluorescence spectra (OD ≈ 0.15 for **1** at the excitation wavelength of ~420 nm) in TFE (red), MeOH (blue), and 10% MeOH/H_2O (green). (b) Time-resolved fluorescence spectra of H_2TPP in THF (purple) and **1** in 100% TFE (red), 100% MeOH (blue), and IRF (black) with 580 nm excitation and detection at an emission wavelength of 650 or 690 nm (OD ≈ 0.15 at 580 nm).

The couplet at 240 nm emerges from transitions polarized along the short axis of the NDI, indicating the presence of a *P*-type intermolecular helical orientation.[16] The couplet corresponding to the porphyrin Soret band at 428 nm is associated with two quasi-degenerate transitions, oriented perpendicular to each other. However, since rotation of the porphyrin is possible only around the long axis of **1**, an effective transition dipole moment along this axis can be used to describe the excitonic coupling of the Soret band.[17] Accordingly, the positive chirality of the couplet indicates a *P*-type helicity relating the porphyrins within the assembly.

In contrast, no CD signals were present in TFE, and only the porphyrin Soret band exhibited an excitonic couplet at 428 nm of the CD spectrum under conditions (MeOH, 10% MeOH/H_2O, pH 1 and 13) that produced disordered, amorphous aggregates, as observed by TEM (Figures 3b and S7). The lack of any NDI-related peaks in the CD spectra suggests that intermolecular porphyrin $\pi-\pi$ interactions exclusively drive assembly under these conditions, resulting in disordered NDI segments within the assembly that do not display CD signals. This observation is consistent with the well-known tendency of porphyrin molecules to spontaneously aggregate into amorphous materials.[9a] Conversely, under conditions promoting nanotube formation (10% MeOH/H_2O, pH 7), excitonic couplets due to both the NDI and porphyrin segments indicate that NDI−NDI and porphyrin−porphyrin $\pi-\pi$ interactions contribute to formation and stability of the initial monolayer that precedes nanotube formation.

Self-Assembly Mechanism. A model for the self-assembly of bolaamphiphile **1** can be envisaged as shown in Figure 4. In 10% MeOH/H_2O, monolayer formation precedes formation of the nanorings, which then stack into nanotubes. This assembly process is readily apparent by AFM imaging in which various stages of ring stacking and nanotube maturing can be observed (Figure 2). The monolayer is stabilized by extensive intermolecular $\pi-\pi$ interactions. At high or low pH in 10% MeOH/H_2O, charge−charge repulsive interactions among the head groups likely impede the formation of NDI−NDI stacks and disrupt monolayer formation. Thus, a nonspecific assembly process driven by porphyrin $\pi-\pi$ interactions predominates under these conditions. Given the increased hydrophobicity **1**, the resemblance of this process to the nanotube assembly of NDI−dilysine is noteworthy. The tendency of **1** to form multilamellar nanotubes appears to be the primary consequence of the greater hydrophobicity.

Time-Resolved Spectroscopy. In order to assess how the propensity of **1** to undergo photoinduced electron transfer varies with the nature of the assembly, a combination of steady-state and time-resolved fluorescence spectroscopy and ultrafast femtosecond pump−probe transient absorption experiments were performed under different solvent conditions. Steady-state fluorescence measurements of **1** were characterized by two emission bands for the porphyrin at 650 and 720 nm upon excitation (λ_{ex}) of the porphyrin at 420 nm, and at ~390 and 450 nm with excitation of the NDI group at 360 nm (Figures 5a, S8, and S9). The fluorescence spectrum of dialkyl-substituted NDIs is characterized by emission bands at 390, 410, and 430 nm, depending upon substitution.[18] The red-shifted fluorescence bands observed here are consistent with NDI aggregation.[8,19] Fluorescence quantum yield measurements in 100% MeOH with excitation of the porphyrin at λ_{ex} = 420 nm resulted in $\Phi_{Fl} \approx 0.0003$ for the porphyrin fluorescence, while in TFE, a solvent in which **1** is only minimally aggregated, we observed $\Phi_{Fl} \approx 0.005$. Both values are significantly smaller than the Φ_{Fl} of H_2TPP[20] and are consistent with either photoinduced electron transfer from the electronically excited porphyrin to an NDI, or aggregation-induced fluorescence quenching of the TPP excited state.[21,22] Fluorescence experiments in 10% MeOH/H_2O resulted in a fluorescence signal

dx.doi.org/10.1021/ja205868b |*J. Am. Chem. Soc.* 2011, 133, 19125–19130

too small to quantify accurately. Attempts to quantify the fluorescence quantum yields from the excited NDIs were also unsuccessful, although the NDI fluorescence intensities measured in 100% MeOH and TFE are 2−5 fold greater than that measured in 10% MeOH/H_2O.

Time-correlated single-photon counting (TCSPC) experiments in 100% MeOH with 580 nm excitation yielded a decay best fit to a triexponential decay, with lifetime (τ_{Fl}) components of 1.96 ns (19%), 389 (63%), and 72 ps (18%) (Figure 5b). Similarly short lifetimes were observed in TFE, where a long-lived component of 1.46 ns (10%) and two short-lived components of 208 ps (32%) and 32 ps (58%) were observed. We were unable to determine any lifetime data in 10% MeOH/H_2O with λ_{ex} = 580 nm as a result of the low amount of fluorescence from the porphyrin moiety in this solvent. TCSPC experiments were also performed with λ_{ex} = 320 nm, where >98% of the incident light is absorbed by the NDI group (Figures S9 and S10). The reported lifetime for a monomeric, disubstituted NDI is 16 ps;[18] however, we have previously reported significant enhancements in the NDI lifetime upon aggregation and nanotube/nanotape formation, with lifetimes sometimes >200 ps depending on the nature of the assembly.[8,19a] These long lifetimes correspond to delocalization of the excited-state energy over several NDI units in the assembly, and in some cases they were accompanied by energy migration through the assembly.[8] In 100% TFE, largely single-exponential decays of ∼25 and 29 ps,[18] with a minor (∼3−8%) component with a lifetime of 233−265 ps, were observed at the NDI emission bands at 382 and 450 nm, respectively. Two components to the fluorescence decay profiles at each wavelength were also observed in 100% MeOH, with the short-lived component having a lifetime of τ_{Fl} = 20−30 ps (85%) and the longer component with τ_{Fl} = 206−225 ps (11−13%). Although **1** is predominantly monomolecular in TFE, as evidenced by UV, CD, and TEM/AFM imaging, small amounts of aggregates are likely to be present. Consequently, the long-lived components of these decays are consistent with the fluorescence of aggregated NDIs. In contrast, excitation of the NDI group of **1** in 10% MeOH/H_2O yielded only one short-lived component, having τ_{Fl} = 45 ps (99%). The monoexponential lifetime recorded in 10% MeOH/H_2O is considerably shorter than for other highly assembled NDI chromophores,[8,19] and is different than the lifetimes for **1** recorded in either TFE or 100% MeOH.

Time-resolved fluorescence anisotropy experiments on **1** were performed in MeOH and TFE. The initial anisotropy (r_0) for H_2TPP, for which the fluorescence signal depolarizes rapidly in solution by free rotation, was found to be ∼0.06 in THF, consistent with the literature value of 0.11.[23] Values of r_0 for **1** with 580 nm excitation in MeOH (0.34) and TFE (0.35) were comparable to one another and to data collected with 320 nm excitation and emission monitoring at 450 nm (0.31 in MeOH and 0.23 in TFE). The relatively large r_0 values are consistent with the lack of energy migration from either porphyrin or NDI excited states in these solvents.[8]

Femtosecond transient absorption experiments were performed on **1** with λ_{ex} = 360 nm, where the NDI chromophore absorbs the majority of the incident photons. Experimental limitations on the concentration necessary for nanotube formation and laser power prevented the acquisition of usable data with λ_{ex} = 420 or 580 nm, respectively. Excitation in TFE with 360 nm light produced a transient signal at early time delays characterized by three broad absorption bands centered at 460, 490, and 620 nm

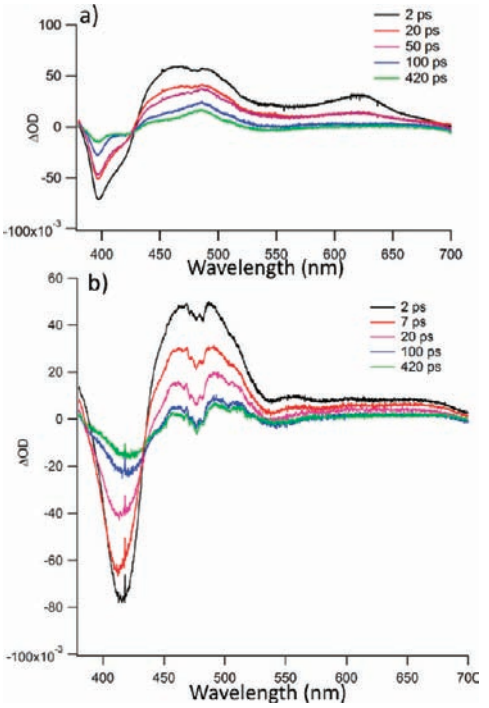

Figure 6. Transient absorption spectra of 0.2 mM solutions of **1** in (a) TFE and (b) 10% MeOH/H_2O following a 360 nm, 40 fs laser flash.

that grew in with the laser pulse and were accompanied by negative absorptions at 400 and 420 nm (Figure 6a). The negative band at 400 nm corresponds to stimulated emission of the NDI fluorescence, while the 420 nm band is indicative of the bleach from the porphyrin Soret band. The decay profiles of the 400 nm stimulated emission and the 460, 490, and 620 nm decays were all similar (τ = 15−18 ps) to one another, indicating they arise from the same transient species. After ∼30 ps these bands had decayed and were replaced with another transient absorption band at 485 nm and a weak and very broad absorption band at 570−680 nm. The rise time of these transients could not be determined because their signals are superimposed upon the early-time bands in the 460−490 and 620 nm regions. The bands at 485 and 570−680 nm were observed to decay on significantly longer time scales than the other absorption bands and exceeded the experimental time window of 3 ns. Nearly identical results were obtained in 100% MeOH, although the initial decay times at all wavelengths were on the order of 6−9 ps (Figure S11). The band at 485 nm decayed with a lifetime of ∼1.4 ns in this solvent. The transient absorption bands at 460, 490, and 620 nm are all consistent with the NDI singlet excited state. The low-energy band has been observed at slightly higher energies (∼606 nm) in previous experiments,[24] but aggregation in both solvents most likely leads to a red-shifted band. The lifetimes measured at these wavelengths are similar to the short lifetimes obtained in the TCSPC experiments, and are consistent with excited-state decay and charge separation. The presence of the long-lived band at 485 nm is consistent with the presence of the NDI radical anion, which has a prominent absorption at this wavelength. The NDI radical anion also has an absorption band at 620 nm,[25,26] and the appearance of a broad feature in the transient absorption spectrum at the same time as the 485 nm band indicates they both arise from the NDI radical anion. Wasielewski and co-workers have reported that a delocalized charge-separated state

in porphyrin-perylenediimide (PDI) showed the delocalized PDI radical anion to broaden significantly with increased stacking interactions.[27] The fact that we do not observe charge recombination on the time scale of these experiments is also consistent with that work, where delocalization of radical anions led to longer-lived charge separation.

The transient absorption spectra in 10% MeOH/H_2O are different than in either MeOH or TFE (Figure 6b). In these spectra, the absorption bands at 485 and 570−680 nm that are attributed to the NDI radical anion are absent, as is the low-energy band of the NDI excited state at 620 nm. The stimulated emission band at 400 nm appears to have merged with the Soret bleach, which has shifted to 430 nm. Only the NDI excited-state bands at 460 and 495 nm are clearly evident. The decays at 460 and 495 nm were best fit to triexponential decays and showed two major components with lifetimes of ∼3−4 and ∼50 ps, and a minor component (<10%) of ∼1.5 ns lifetime. The lifetime component of 50 ps is nearly identical to the fluorescence lifetime (45 ps) obtained from TCSPC experiments. The close correlation of the TCSPC value and the 50 ps transient absorption value is consistent with decay of the NDI excited state and may be attributed to electron transfer from the porphyrin to the electronically excited NDI.

The lack of an observable NDI radical anion signal at 485 or 570−680 nm can be rationalized using two alternative kinetic scenarios. One interpretation would suggest that charge separation in 10% MeOH/H_2O (∼45−50 ps) is slower than in either 100% MeOH or TFE, and the lifetime of the charge-separated state is significantly shorter-lived. The ultrafast component of 3−4 ps would then reflect the rate of charge recombination. However, previous picosecond fluorescence experiments indicate that NDI nanotube assemblies exhibit long-lived NDI excited states[8] that often are accompanied by rapid migration of the excited-state energy. Therefore, it is also quite possible that the radical anion has similar mobility/delocalization, which would then be expected to result in a longer-lived charge-separated state. The extensive delocalization of the radical anion within the nanotube $\pi-\pi$ arrays would be expected to result in extensive broadening of the radical anion bands in the transient absorption spectra, consistent with the broad feature observed in the range 550−650 nm in the transient spectra. Indeed, Wasielewski and co-workers have demonstrated long-lived charge separation in stacked porphyrin−PDI assemblies where the radical anion was delocalized over several units in the assembly. With these observations in mind, the two time constants we observe in the transient absorption experiments likely emerge from different charge-separation events, one with a time constant of 3−4 ps and another with 45−50 ps, the latter of which is observed in the TCSPC experiments and the former too fast to resolve on our TCSPC instrument. The third, longer-lived component present in the decay represents charge recombination but is too long-lived (τ > 1.5 ns) to be fit accurately. Although these kinetic scenarios cannot be unambiguously distinguished, the observation of two time constants for electron transfer is consistent with the nanotube structure. Our prior solid-state NMR studies of an NDI nanotube identified very different conformational dynamics in the interior and exterior environments of the nanotubes, and these two regions could be distinguished spectroscopically.[8] Hence, the two time constants for electron transfer may arise from the different positioning of the two NDI chromophores with respect to the interior and exterior nanotube surfaces.

CONCLUSION

We have described the bolaamphiphilic self-assembly of a donor/acceptor dyad, **1**, into 1D nanotubes containing a supramolecular heterojunction. The nanotubes form via extensive intermolecular $\pi-\pi$ interactions between the NDI and TPP chromophores. Transient absorption spectra in TFE and MeOH reflect the generation of charge-separated states. The transient spectra of nanotubes of **1** formed in 10% MeOH/H_2O are very different from those in TFE and MeOH. Notably, nanotube structure results in very different photophysics compared with nonspecific or minimally aggregated forms of **1**. This work demonstrates the importance of controlling local nanostructure in modulating the photophysical properties of optoelectronic materials.

ASSOCIATED CONTENT

Supporting Information. Experimental details, TEM and AFM images, CD, NMR, MS, and UV spectra, fluorescence data, and transient absorption spectra/decay profiles for bolaamphiphile **1**. This material is available free of charge via the Internet at http://pubs.acs.org.

AUTHOR INFORMATION

Corresponding Author
dmodarelli@uakron.edu; parquett@chemistry.ohio-state.edu

ACKNOWLEDGMENT

This work was supported by the National Science Foundation (CHE-1057884, CRC-0526864 and CHE-0216371). We acknowledge the technical assistance and usage of the AFM core facility at Davis Heart and Lung Research Institute, and Michael Severance and Lynetta Mier in the Ohio State Center for Chemical and Biophysical Dynamics for their assistance with the transient absorption experiments.

REFERENCES

(1) (a) Bhosale, R.; Misek, J.; Sakai, N.; Matile, S. *Chem. Soc. Rev.* **2010**, *39*, 138. (b) Brabec, C. J.; Sariciftci, N. S.; Hummelen, J. C. *Adv. Funct. Mater.* **2001**, *11*, 15. (c) Zhao, X.; Zhan, X. *Chem. Soc. Rev.* **2011**, *40*, 3369.

(2) (a) Peumans, P.; Yakimov, A.; Forrest, S. R. *J. Appl. Phys.* **2003**, *93*, 3693. (b) Halls, J. J. M.; Walsh, C. A.; Greenham, N. C.; Marseglia, E. A.; Friend, R. H.; Moratti, S. C.; Holmes, A. B. *Nature* **1995**, *376*, 498. (c) Yu, G.; Gao, J.; Hummelen, J. C.; Wudl, F.; Heeger, A. J. *Science* **1995**, *270*, 1789. (d) Sariciftci, N. S.; Smilowitz, L.; Heeger, A. J.; Wudl, F. *Science* **1992**, *258*, 1474. (e) Peumans, P.; Uchida, S.; Forrest, S. R. *Nature* **2003**, *425*, 158.

(3) (a) Zang, L.; Che, Y. K.; Moore, J. S. *Acc. Chem. Res.* **2008**, *41*, 1596. (b) Hoeben, F. J. M.; Jonkheijm, P.; Meijer, E. W.; Schenning, A. P. H. J. *Chem. Rev.* **2005**, *105*, 1491. (c) Grimsdale, A. C.; Müllen, K. *Angew. Chem., Int. Ed.* **2005**, *44*, 5592. (d) Facchetti, A.; Usta, H.; Marks, T. J. *Acc. Chem. Res.* **2011**, *44*, 501.

(4) (a) Coropceanu, V.; Cornil, J.; da Silva, D. A.; Olivier, Y.; Silbey, R.; Bredas, J. L. *Chem. Rev.* **2007**, *107*, 926. (b) Wasielewski, M. R. *Acc. Chem. Res.* **2009**, *42*, 1910.

(5) (a) Würthner, F.; Chen, Z. J.; Hoeben, F. J. M.; Osswald, P.; You, C. C.; Jonkheijm, P.; von Herrikhuyzen, J.; Schenning, A. P. H. J.; van der Schoot, P. P. A. M.; Meijer, E. W.; Beckers, E. H. A.; Meskers, S. C. J.; Janssen, R. A. J. *J. Am. Chem. Soc.* **2004**, *126*, 10611. (b) Jonkheijm, P.; Stutzmann, N.; Chen, Z. J.; de Leeuw, D. M.; Meijer, E. W.; Schenning, A. P. H. J.; Wurthner, F. *J. Am. Chem. Soc.* **2006**, *128*, 9535. (c) Li, W. S.; Yamamoto, Y.; Fukushima, T.; Saeki, A.; Seki, S.; Tagawa, S.; Masunaga,

H.; Sasaki, S.; Takata, M.; Aida, T. *J. Am. Chem. Soc.* **2008**, *130*, 8886. (d) Sisson, A. L.; Sakai, N.; Banerji, N.; Furstenberg, A.; Vauthey, E.; Matile, S. *Angew. Chem., Int. Ed.* **2008**, *47*, 3727. (e) Kira, A.; Umeyama, T.; Matano, Y.; Yoshida, K.; Isoda, S.; Park, J. K.; Kim, D.; Imahori, H. *J. Am. Chem. Soc.* **2009**, *131*, 3198. (f) Kishore, R. S. K.; Kel, O.; Banerji, N.; Emery, D.; Bollot, G.; Mareda, J.; Gomez-Casado, A.; Jonkheijm, P.; Huskens, J.; Maroni, P.; Borkovec, M.; Vauthey, E.; Sakai, N.; Matile, S. *J. Am. Chem. Soc.* **2009**, *131*, 11106. (g) Gorodetsky, A. A.; Chiu, C.-Y.; Schiros, T.; Palma, M.; Cox, M.; Jia, Z.; Sattler, W.; Kymissis, I.; Steigerwald, M.; Nuckolls, C. *Angew. Chem., Int. Ed.* **2010**, *49*, 7909. (h) Hizume, Y.; Tashiro, K.; Charvet, R.; Yamamoto, Y.; Saeki, A.; Seki, S.; Aida, T. *J. Am. Chem. Soc.* **2010**, *132*, 6628. (i) Che, Y.; Huang, H.; Xu, M.; Zhang, C.; Bunes, B. R.; Yang, X.; Zang, L. *J. Am. Chem. Soc.* **2011**, *133*, 1087.

(6) Dresselhaus, G.; Dresselhaus, M. S.; Jorio, A. *Carbon nanotubes: advanced topics in the synthesis, structure, properties, and applications*; Springer: Berlin/New York, 2008.

(7) (a) Yamamoto, Y.; Zhang, G. X.; Jin, W. S.; Fukushima, T.; Ishii, N.; Saeki, A.; Seki, S.; Tagawa, S.; Minari, T.; Tsukagoshi, K.; Aida, T. *Proc. Natl. Acad. Sci. U.S.A.* **2009**, *106*, 21051. (b) Yamamoto, Y.; Fukushima, T.; Suna, Y.; Ishii, N.; Saeki, A.; Seki, S.; Tagawa, S.; Taniguchi, M.; Kawai, T.; Aida, T. *Science* **2006**, *314*, 1761.

(8) Shao, H.; Seifert, J.; Romano, N. C.; Gao, M.; Helmus, J. J.; Jaroniec, C. P.; Modarelli, D. A.; Parquette, J. R. *Angew. Chem., Int. Ed.* **2010**, *49*, 7688.

(9) (a) Drain, C. M.; Varotto, A.; Radivojevic, I. *Chem. Rev.* **2009**, *109*, 1630. (b) Liu, H. B.; Xu, J. L.; Li, Y. J.; Li, Y. L. *Acc. Chem. Res.* **2010**, *43*, 1496.

(10) (a) Shioi, A.; Hatton, T. A. *Langmuir* **2002**, *18*, 7341. (b) Shao, H.; Parquette, J. R. *Molecular Recognition and Polymers*; John Wiley & Sons, Inc.: New York, 2008; p 259. (c) Shimizu, T.; Masuda, M.; Minamikawa, H. *Chem. Rev.* **2005**, *105*, 1401.

(11) (a) Luguya, R.; Jaquinod, L.; Fronczek, F. R.; Vicente, M. G. H.; Smith, K. M. *Tetrahedron* **2004**, *60*, 2757. (b) Meng, G. Z. G.; James, B. R.; Skov, K. A. *Can. J. Chem.* **1994**, *72*, 1894.

(12) Zhou, Y. *Crit. Rev. Solid State Mater. Sci.* **2008**, *33*, 183.

(13) (a) Reches, M.; Gazit, E. *Science* **2003**, *300*, 625. (b) Shao, H.; Parquette, J. R. *Angew. Chem., Int. Ed.* **2009**, *48*, 2525. (c) Matsumura, S.; Uemura, S.; Mihara, H. *Mol. Biosyst.* **2005**, *1*, 146.

(14) Okada, S.; Segawa, H. *J. Am. Chem. Soc.* **2003**, *125*, 2792.

(15) (a) Würthner, F. *Chem. Commun.* **2004**, 1564. (b) Schenning, A. P. H. J.; Jonkheijm, P.; Peeters, E.; Meijer, E. W. *J. Am. Chem. Soc.* **2001**, *123*, 409.

(16) Gawronski, J.; Brzostowska, M.; Kacprzak, K.; Kolbon, H.; Skowronek, P. *Chirality* **2000**, *12*, 263.

(17) Pescitelli, G.; Gabriel, S.; Wang, Y. K.; Fleischhauer, J.; Woody, R. W.; Berova, N. *J. Am. Chem. Soc.* **2003**, *125*, 7613.

(18) Posokhov, Y.; Alp, S.; Koez, B.; Dilgin, Y.; Icli, S. *Turk. J. Chem.* **2004**, *28*, 415.

(19) (a) Shao, H.; Nguyen, T.; Romano, N. C.; Modarelli, D. A.; Parquette, J. R. *J. Am. Chem. Soc.* **2009**, *131*, 16374. (b) Shao, H.; Parquette, J. R. *Chem. Commun.* 2010, *46*, 4285.

(20) Strachan, J. P.; Gentemann, S.; Seth, J.; Kalsbeck, W. A.; Lindsey, J. S.; Holten, D.; Bocian, D. F. *J. Am. Chem. Soc.* **1997**, *119*, 11191.

(21) Serpone, N.; Khairutdinov, R. F. *J. Phys. Chem. B* **1999**, *103*, 761.

(22) Wang, Z. C.; Medforth, C. J.; Shelnutt, J. A. *J. Am. Chem. Soc.* **2004**, *126*, 15954.

(23) Maiti, N. C.; Mazumdar, S.; Periasamy, N. *J. Phys. Chem.* **1995**, *99*, 10708.

(24) Zuilhof, H.; Ganesan, P.; Baggerman, J.; Zhang, H.; Sudholter, E. J. R. *J. Phys. Chem. A* **2007**, *111*, 6151.

(25) Gosztola, D.; Niemczyk, M. P.; Svec, W.; Lukas, A. S.; Wasielewski, M. R. *J. Phys. Chem. A* **2000**, *104*, 6545.

(26) Imahori, H.; Okamoto, K.; Mori, Y.; Yamada, H.; Fukuzumi, S. *Chem. Commun.* **2004**, *10*, 474.

(27) van der Boom, T.; Hayes, R. T.; Zhao, Y. Y.; Bushard, P. J.; Weiss, E. A.; Wasielewski, M. R. *J. Am. Chem. Soc.* **2002**, *124*, 9582.